A simple method for the preliminary analysis and benchmarking of automotive LiDARs in fog

1st Davide Cassanelli
Dep. of Engineering "E. Ferrari"
University of Modena and R. Emilia
Modena, Italy
davide.cassanelli@unimore.it

2nd Stefano Cattini
Dep. of Engineering "E. Ferrari"
University of Modena and R. Emilia
Modena, Italy
stefano.cattini@unimore.it

3rd Giorgio Di Loro
Dep. of Engineering "E. Ferrari"
University of Modena and R. Emilia
Modena, Italy
giorgio.diloro@unimore.it

4th Luca Di Cecilia
CNH Industrial S.p.a.
Modena, Italy
luca.dicecilia@cnhind.com

5th Luca Ferrari
CNH Industrial S.p.a.
Modena, Italy
luca.ferrari@cnhind.com

6th Daniele Goldoni
Dep. of Engineering "E. Ferrari"
Uni. of Modena and R. Emilia
Modena, Italy
daniele.goldoni@unimore.it

7th Luigi Rovati
Dep. of Engineering "E. Ferrari"
Uni. of Modena and R. Emilia
Modena, Italy
luigi.rovati@unimore.it

***Abstract*—The vast multitude of LiDAR systems currently available on the market makes the need for methods to compare their performances increasingly high. In this study, we focus our attention on the development of a method for the analysis of the effects induced by the fog, one of the main challenges for Advanced Driver Assist Systems (ADASs) and autonomous driving. Large experimental setups capable of reconstructing adverse weather conditions on a large scale in a controlled and repeatable way are certainly the best test conditions to analyze and compare LiDARs performances in the fog. Nonetheless, such large plants are extremely expensive and complex, therefore only available in a few sites in the world. In this study, we thus propose a measurement method, a data analysis procedure and, an experimental setup that are extremely simple and inexpensive to implement. The achievable results are reasonably less accurate than those obtainable with large plants. Nevertheless, the proposed method can allow to easily and quickly obtain a preliminary estimate of the performance in the presence of fog and a rapid benchmarking of different LiDAR systems.**

***Index Terms*—LiDAR, Fog, Bad weather conditions, Automotive measurement, Autonomous driving, ADAS.**

I. Introduction

Autonomous driving is considered to be a game changer for future mobility. The resulting strong interest has brought to a vast multitude of LiDAR systems available on the market making the need for methods to compare their performances ever more pressing. In response to this, several studies have been recently proposed e.g. [1]–[6]. Most of such studies have focused on the performances obtainable in conditions of good visibility, that is, when the transmission medium, the air, has no or negligible absorption and scattering. Adverse environmental conditions such as, for example, fog, rain, and snow, can strongly modify the optical properties of the transmission medium and, therefore, have a very severe impact on the performance of LiDARs.

In this study, we focus our attention on the effects induced by the fog. The best way to experimentally analyze the behavior of a LiDAR in the presence of fog is reasonably to immerse the LiDAR and the target inside an environment with a known, uniform, and constant level of fog. Since LiDARs for automotive applications typically operate with targets located at distances ranging from a few meters to several tens of meters, the realization of such an experimental setup is extremely complex and expensive. Examples of large experimental setups that allow both LiDAR and target to be immersed within a wide foggy environment are the CEREMA's Adverse Weather Facility in Clermont-Ferrand, France and, the weather chamber at the Japan Automobile Research Institute (JARI) in Tsukuba, Japan. Examples of LiDARs characterization obtained using the CEREMA's Adverse Weather facility have been published by Kutila *et al.* [7].

In this study, we propose a measurement method, a data analysis procedure, and an experimental setup that are extremely simple and inexpensive to implement. The goal is to obtain an extremely simple and economical testbed that allows obtaining an estimate, albeit approximate, of the LiDARs performances in the presence of fog, thus allowing a preliminary benchmarking. The proposed setup does not require immersing the LiDAR and the target inside an environment in which all the optical path that separates them is filled with fog. On the contrary, the fog is confined only within a compartment — the fog chamber — which is interposed between the LiDAR and the target, thus allowing to analyze targets at considerably greater distances than the size of the fog chamber.

In the following, section II recalls the theoretical framework and describes the setup and measurement procedure proposed for the analysis of the effects of fog. By way of example, section III reports some results obtained analyzing the performance of a commercial LiDAR (model MRS 6000, by Sick). Finally, section IV briefly analyzes the obtained results and discusses strengths and limitations of the proposed method.

II. Materials and methods

A. Theoretical framework and proposed simplified model

The intensity of the current pulse generated by the LiDAR detector depends on the integral of the radiance within the field of view (FOV) of its aperture.
Adverse environmental conditions such as fog, rain, and snow, can strongly modify the optical properties of the transmission medium, thus modifying the radiance of both the beams generated by the LiDAR and the one reflected by the target. As a result, such adverse environmental conditions may have a severe impact on the performance of 3D-LiDARs.

The exact calculation of the power that reaches the detector requires the solution of the time-resolved radiative transfer equation resulting extremely complex and not always solvable in an analytical form. Indeed, light propagation in scattering and adsorbing media such as fog, rain, and snow is a multiple-scattering propagation in which photons undergo many scattering events before reaching the aperture of the LiDAR detector or, being absorbed by the transmission medium or the surrounding environment.

Given that, in many practical cases, the solution of the radiative transfer equation is substantially impossible, over the years, innumerable models have been developed to describe light propagation in dense medium aerosols.
A simple but useful parameter often used to describe the attenuation of light caused by its propagation through fog is the meteorological optical range (MOR) [8].
Recalling the definitions proposed by the World Meteorological Organization (WMO) [8], the ISO 28902-1:2012 standard [9], defines the MOR (for propagation through fog droplets) as: "*length of path in the atmosphere required to reduce the luminous flux in a collimated beam from an incandescent lamp, at a colour temperature of 2700 K, to 5% of its original value*". Then, although the collimated beam will tend to smear during propagation within the fog, its attenuation is modeled using the Lambert-Beer law (also known as Bouguer-Lambert law) [8], [9]. According to the Lambert–Beer law, which provides an exact estimate of the attenuation only in the case of a purely absorbing medium, the irradiance of a monochromatic and collimated beam of radiation that propagates along the z-axis is given by [10]:

$$E(z) = E(0) \cdot \exp\left[- \int_z \sigma(z)\ \mathrm{d}z \right] , \tag{1}$$

where $E(z)$ is the irradiance at z, $E(0)$ is the irradiance at $z = 0$ and, $\sigma(z)$ is the extinction coefficient per unit length at z. If the medium is homogeneous, the Lambert-Beer law reduces to the classical form:

$$E(z) = E(0) \cdot \exp(-\sigma \cdot z) , \tag{2}$$

and, based on its definition, the MOR can be calculated as [8], [9]:

$$0.05 = \exp(-\sigma \cdot \mathrm{MOR}) \Rightarrow \mathrm{MOR} = \frac{1}{\sigma} \ln \frac{1}{0.05} \approx \frac{3}{\sigma} , \tag{3}$$

In the proposed method, the MOR will be used to provide an estimate, albeit rough, of the fog level inside the fog chamber.

B. The proposed setup

To greatly simplify the complexity of the test setup, the proposed method confines the fog only in a section of the optical path that separates the LiDAR under test (instrument under test — IUT) and the target. Actually, the scattering centers — the droplets of fog — modify the radiation pattern both in terms of intensity and angular distribution. Therefore, the result obtained will not be exactly the same as that which would have been obtained by inserting the IUT and the target inside an environment in which the concentration of fog is uniform and constant along the entire optical path. However, note that, within the validity of the Lambert-Beer law approximation, from (1) the attenuation due to propagation through a medium of thickness d and extinction coefficient σ is the same as that which would occur crossing two media of thickness $d/2$ each, one of which having extinction coefficient 0 and, the other, extinction coefficient 2σ. Therefore, in the approximation of considering the Lambert-Beer law applicable, the fog chamber allows to adequately model the effect of the fog.

As shown in Fig. 1, the proposed simplified setup is thus based on a fog chamber positioned along the optical path between the IUT and the target and feed by an ultrasonic mist maker. The fog is produced in the fog generation chamber, FGC, and then pumped towards the fog chamber, FC, using a fan that conveys the generated fog into a tube. As shown in Fig. 2, the roof of the FC has nozzles that diffuse the fog. The bottom of the FC has small openings on the sides that allow venting the airflow pumped from the fog generation chamber. The use of two separate chambers, that is, the FGC and the FC, allowed to obtain a better uniformity of the fog compared to that which was obtained by generating the fog directly inside the FC. Since the size of the droplets determines their optical properties, the particle sizing of the fog in the FC was analyzed through dynamic light scattering (DLS), highlighting an average diameter of 6 μm, therefore, consistent with the size of natural fog droplets [11].

As shown in Fig. 2, to allow the LiDAR beams to pass, the fog chamber has two optically transparent windows (as described in subsection II-C, the proposed method involves analyzing only one of the beams generated by the IUT). To avoid the LiDAR detector collecting the echoes due to specular reflections from such transparent walls, the fog chamber is tilted by an angle α to the normal to the optical axis (z-axis) of the LiDAR (see Fig. 1). The attenuation introduced by the fog chamber is estimated using a laser diode, LD (model MLS-6X10 by Optical Fiber Systems, INC.), having a wavelength as close as possible to that of the IUT (the examples shown in section III were obtained using a LD with a wavelength of 904 nm — the IUT wavelength was 870 nm). The beam generated by LD is collimated and its optical power is measured using a photodiode, PD (model S1223 by Hamamatsu), having an active area wider than the LD laser spot. The setup also includes a grayscale camera (camera model EO-1312 by Edmund Optics, lens model HF12.5SA-1 by Fujinon) aimed at providing a (coarse) estimate of the

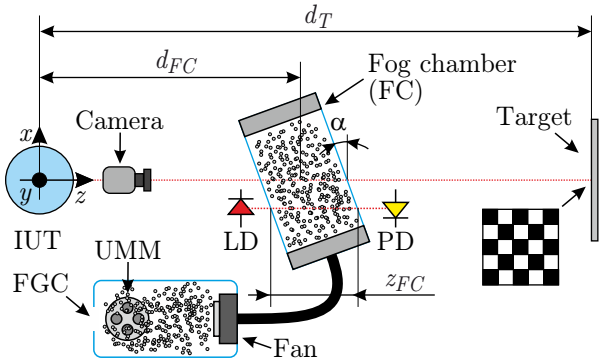

Fig. 1. Schematic representation of the proposed setup. The fog is generated by the ultrasonic mist maker, UMM, and pumped by the fan positioned inside the fog generation chamber, FGC. Feed by the FGC, the fog chamber, FC, is positioned to interpose itself between the IUT and the target. To avoid the LiDAR collecting the echoes due to specular reflections from the transparent walls of the FC, it is tilted by an angle α to the normal to the optical axis (z-axis) of the LiDAR. The optical path length of the IUT inside the FC, z_{FC}, is therefore increased by a factor of $1/\cos\alpha$ compared to the FC depth. The laser diode, LD, and the photodiode, PD, allow estimating the attenuation introduced by the fog chamber. The grayscale camera is aimed at providing an estimate of the visibility that the driver would have when looking through the fog. To allow this, the target was made using a white paper sheet on which a checkerboard of black rectangles was printed. d_T is the distance between the IUT and the target, while d_{FC} is the distance between the IUT and the FC center.

visibility that the driver would have when looking through the fog. As will be described in subsection II-C, the camera must be aligned with the LiDAR beam used in the analysis. Furthermore, the part of the target framed by the camera must have a pattern that allows the estimation of the contrast. In our case, a checkerboard with black and white rectangles was used.

The example results reported in section III have been obtained setting a LiDAR to target distance d_T = 1.15 m, a LiDAR to fog chamber distance $d_{FC} \approx 0.80$ m and tilt angle $\alpha = 20°$. The whole system was mounted on an aluminum optical rail which allowed the various elements to be aligned and held in position.

C. Proposed procedure and data analysis

The proposed method involves analyzing the estimate of the position of the fixed target as the concentration of fog inside the fog chamber varies. The error introduced by the IUT in the estimate is then analyzed both in relation to the attenuation and the reduction in visibility caused by fog. The fewer the variations in the indications provided by the IUT, the greater the robustness of the IUT against fog.

To provide an indication, albeit qualitative, of the fog level, the errors are also analyzed as a function of the MOR defined in (3). The proposed method thus involves the periodic and synchronous acquisition of the following quantities with sampling frequency f_C:

1) a point cloud, PC, by the IUT,
2) an estimate of the attenuation using LD and PD,
3) an estimate of the visibility using the camera.

After waiting for the warm-up of all the systems involved, the proposed procedure entails acquiring the first n_{base} acquisitions before starting pumping fog inside the FC. Such acquisitions serve as a baseline both for the attenuation and visibility. Then, the procedure involves starting pumping the fog inside the fog chamber. The procedure ends once n_{TOT} acquisitions have been acquired for each of the three systems — the IUT, the LD and PD and, the camera. Such a procedure has to be repeated n_{rep} times.

The example results that will be shown in section III have been obtained with $f_C \approx 1$ Hz, n_{base} = 10, n_{TOT} = 300 and, n_{rep} = 15.

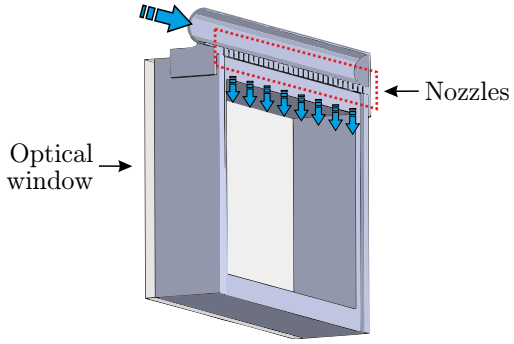

Fig. 2. Section of the fog chamber. The large arrow (blue in the color version) represents the flow of fog coming from the FGC. The smaller arrows represent the flow of fog that spreads into the chamber. The internal dimensions of the chamber are 10 cm both for the width and for the height, and 5 cm for the depth (the depth along the optical axis of the IUT is increased by a factor of $1/\cos\alpha$). The body of the fog chamber was made in PLA (polylactic acid) through 3D printing. In the figure, it is possible to see the nozzles from which the fog generated in the fog generation chamber is diffused (nozzle diameter 1 mm, inter-distance between nozzles 5 mm). The optical windows are two 5 mm thick polycarbonate sheets.

For each acquired PC, the proposed procedure involves analyzing only one of the beams generated by the IUT. Indeed, LiDARs typically scan the surrounding environment by sampling it along a set of predetermined directions (elevation angle φ and azimuth angle θ) [5]. The proposed method thus involves extracting the value of the radius of the investigated beam — the distance, d, at which the IUT estimates the fixed target. The example results, that will be shown in section III, have been obtained by analyzing the beam with polar coordinate $\theta = 0°$ and, $\varphi = 0°$.

The estimate of the attenuation, A, introduced by the fog chamber is performed by analyzing the current, i, photogenerated by the photodiode. Assuming i_{base} to be the average current recorded during the first n_{base} baseline acquisitions, the attenuation relative to the j^{th} acquisition is calculated in terms of optical absorbance:

$$A(j) = \log_{10}\left[\frac{i_{base}}{i(j)}\right], \tag{4}$$

where A is the absorbance (quantity of dimension one often indicated using the measurement unit "optical density", OD) and, $i(j)$ is the current relating to the j^{th} acquisition. Following the approximation introduced by the WMO [8] and

recalled by ISO 28902-1:2012, such attenuation can be roughly modeled using Lambert Beer's law (which would be valid for purely absorbing media only). Therefore, it is possible to estimate the extinction coefficient within the FC as:

$$\sigma(j) = \frac{A(j)}{\log_{10}(e)} \cdot \frac{1}{z_{FC}} \ , \tag{5}$$

where e is Euler's number and, z_{FC} is the optical path length within FC. The relative meteorological optical range is:

$$\mathrm{MOR}(j) = \frac{1}{\sigma(j)} \ln \frac{1}{0.05} \ . \tag{6}$$

$\mathrm{MOR}(j)$ thus represents the length of the path in a uniform atmosphere having an extinction coefficient equal to $\sigma(j)$, required to reduce the intensity of a monochromatic collimated beam having the same wavelength as the IUT, to 5% of its original value.

The estimate of the visibility that the driver would have when looking through the fog is performed by analyzing the images acquired by the camera. Following a procedure similar to that proposed by the WMO for the estimation of "meteorological visibility in daylight" [8], from each acquired image the contrast is extracted as:

$$C(j) = \frac{B(j) - W(j)}{W(j)} \cdot \frac{1}{C_0} \ , \tag{7}$$

where C is the contrast (quantity of dimension one), $B(j)$ and $W(j)$ are the average values of the gray level relative to the black, B, and white, W, checks acquired in the j^{th} image. C_0 is the average contrast recorded during the first n_{base} baseline acquisitions:

$$C_0 = \frac{1}{n_{base}} \sum_{j=1}^{n_{base}} \frac{B(j) - W(j)}{W(j)} \ . \tag{8}$$

Although the camera has a spectral responsivity that does not match perfectly with the spectral luminous efficiency function, $C(j)$ provides a reasonable estimate of the luminance contrast [12] and, therefore, an estimate of the "meteorological visibility in daylight".

To provide a synthetic representation, the proposed method involves the creation of graphs like the one shown in Fig. 3. For direct time-of-flight (ToF) LiDARs, the radial distance of each point of the PC is a quantized variable that can take on a finite number of values equispaced of the radial quantization step δr [5]. It is, therefore, possible to calculate the empirical probability, $P(d_j, x_i, x_{i+1})$, that the IUT estimates that the target is at distance d_j when the fog level is in the $[x_i, x_{i+1})$ interval. x is the parameter used to describe the fog level, thus, it can be the absorbance A, the contrast C, or the MOR.
Defining Ψ as the set of all the d, A, C, and MOR values recorded during the n_{rep} tests, it is possible to calculate the empirical probability as:

$$P(d_j, x_i, x_{i+1}) = \frac{\mathbf{card}\Big\{\Psi | d = d_j \ \& \ x \in [x_i, x_{i+1})\Big\}}{\mathbf{card}\Big\{\Psi | x \in [x_i, x_{i+1})\Big\}} \ , \tag{9}$$

where $\mathbf{card}\{\ldots\}$ is the cardinality, $\mathbf{card}\{\Psi | d = d_j \ \& \ x \in [x_i, x_{i+1})\}$ is the number of times the distance estimated by the IUT was $d = d_j$ when the fog level was in the $[x_i, x_{i+1})$ interval and, $\mathbf{card}\{\Psi | x \in [x_i, x_{i+1})\}$ is the number of times the recorded fog level was in the $[x_i, x_{i+1})$ interval. Assuming that the distance d_j is the one that best approximates the true target distance d_T, the ideal LiDAR should have a probability equal to 1 for $d = d_j$ regardless of the value of x (and the probability for $d \neq d_j$ should be zero). Actually, as discussed by Cattini *et al.* [5], due to the noise, even in the absence of absorbing and scattering particles along the optical path, the estimate of the target distance provided by real LiDARs is not a deterministic variable but a discrete random variable that can assume the value of a certain number of bins in the proximity of the true target distance. Therefore, even in the absence of fog, in general $P(d \neq d_j) > 0$. However, if the IUT is robust to fog, the probability P should be independent of the value of x. In other words, the value of P inside the cells that compose the synthetic representation shown in Fig. 3 should be constant within each row, thus constant as the fog changes. The greater the deviation from this condition, the lower the robustness of the IUT against fog.

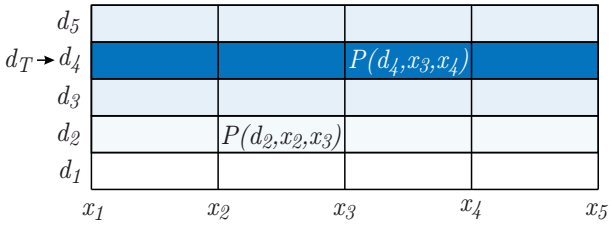

Fig. 3. Conceptual scheme of the proposed synthetic representation. On the x-axis is the parameter used to describe the fog level — the absorbance A, contrast C, or MOR. The x-axis is divided into intervals ranging from the minimum to the maximum value recorded during the tests. On the y-axis, the distance values recorded by the IUT during the tests (for ToF LiDARs the radial distance is quantized — each admitted value constitutes a bin). The numbers inside the cells represent the probability, $P(d_j, x_i, x_{i+1})$, defined in (9), thus representing the probability that the IUT estimates that the target is at that distance d_j when the fog level falls within the $[x_i, x_{i+1})$ range. By way of example, the probabilities $P(d_2, x_2, x_3)$ and $P(d_4, x_3, x_4)$ are shown in the figure. Assuming that the distance d_4 is the one that best approximates the true target distance d_T, the ideal LiDAR should have a probability equal to 1 for all the $d = d_4$ cells regardless of the value of x (and the probability of all cells for $d \neq d_4$ should be zero).

To obtain an estimate, albeit approximate, of the uncertainty associated with the estimate of P, we calculated the experimental standard deviations obtained by analyzing each of the n_{rep} acquisitions individually. In other words, from each of the n_{rep} acquisitions, we calculated the probability

$$P_i(d_j, x_i, x_{i+1}) = \frac{\mathbf{card}\Big\{\psi | d = d_j \ \& \ x \in [x_i, x_{i+1})\Big\}}{\mathbf{card}\Big\{\psi | x \in [x_i, x_{i+1})\Big\}} \ , \tag{10}$$

where ψ is the set d, A, C, and MOR values recorded during the $i \in [1, n_{rep}]$ test. We then calculated the experimental

standard deviation of the arithmetic mean

$$s(d_j, x_i, x_{i+1}) = \sqrt{\frac{1}{n_{rep} \cdot (n_{rep} - 1)} \sum_{i=1}^{n_{rep}} \left(P_i - \bar{P}\right)^2}, \quad (11)$$

where $\bar{P}(d_j, x_i, x_{i+1})$ is the mean $P_i(d_j, x_i, x_{i+1})$.

III. Results

To provide examples of the information that can be obtained using the proposed method, this section reports some results obtained by analyzing the LiDAR model MRS 6000, by Sick. As an example, Fig. 4 shows the trends of: i) the estimate of the target distance, d, obtained from the IUT, ii) the absorbance, A, measured by LD and PD and, iii) the contrast, C, measured by the camera as the concentration of the fog droplets inside the fog chamber increases.

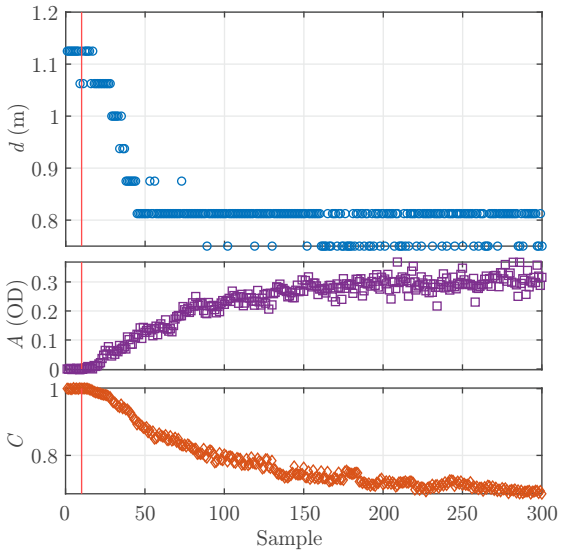

Fig. 4. Typical results of a set of acquisitions. The figure on the top shows the target distance estimated by the IUT (d, ○). The middle figure shows the absorbance measured by LD and PD (A, □) and, the bottom figure shows the contrast measured by the camera (C, ◇). The vertical lines indicate the end of the baseline acquisitions and, therefore, the beginning of the pumping of the fog into the fog chamber.

As described in subsection II-C, for direct ToF LiDARs, the radial distance is a quantized variable that can take on a finite number of values, the bins [5]. As shown in Fig. 4, the quantization step of the IUT is δr = 6.25 cm. Fig. 4 also clearly shows that, as the fog inside the fog chamber increases, the error made by the IUT in estimating the target distance also increases (as described in subsection II-B, measurements were obtained with the target placed at distance d_T = 1.15 m and, the fog chamber placed at distance $d_{FC} \approx 0.8$ m). Furthermore, when the concentration of fog particles exceeds a certain threshold, that is, A large enough or C too small, the IUT is no longer able to correctly reconstruct the target distance, but only reveals the position of the fog front inside the fog chamber.

As described in subsection II-C, to provide a synthetic representation, the proposed method involves calculating the probability P as a function of the fog concentration. Figures 5, 6 and, 7 thus show the values of P as a function of absorbance A, contrast C and, MOR. As described in Fig. 3, the x-axis in Fig.s 5, 6 and, 7 represents the parameter used to describe the fog level — A, C, or the MOR.

The value and the amplitude of the intervals in which to divide the x-axis have to be chosen based on the fog levels of interest for the specific application.
The y-axis represents the bins, the values that the distance estimate can assume. The number inside each cell represents the probability, P, as defined in (9) (top figure) or the experimental standard deviation of the arithmetic mean, s, as defined in (11) (bottom figure). As shown in Fig.s 5, 6 and, 7, as the fog level increases, the MRS 6000 significantly deviates from the ideal LiDAR behavior (for which the probability should be independent of the fog level). Actually, as long as the attenuation $A < 0.01$, that is, the contrast $C > 99\%$ and the MOR> 15.96 m, the bin with the greatest probability is the one whose distance best approximates the distance to the target (bin = 1.125 m, d_T = 1.15 m). As the fog concentration increases, the probability of error increases significantly. When $A > 0.1$, that is, the contrast $C < 90\%$ and the MOR< 1.6 m, the MRS 6000 is no longer able to detect the target, but only reveals the front of the fog inside the fog chamber ($d_{FC} \approx 0.8$ m). A fog bank having such a concentration would then be interpreted by the LiDAR as a target. Consider that fog can reduce the visibility to very few meters and, in extreme cases, down to near zero meters [13]. Therefore, the above fog concentration is not impossible to happen.

IV. Conclusions

The vast multitude of LiDAR systems available on the market makes the need for methods to compare their performances increasingly high. In this study, we focus our attention on a method able to investigate and compare the LiDARs performances in fog. Aware of the fact that an accurate analysis can probably only be obtained through a large setup in which both the LiDAR and the target are completely immersed in the fog, the goal of the proposed method is to create an extremely simple and economical testbed that allows obtaining an estimate, albeit approximate, of the LiDAR performances in the presence of fog. Indeed, large experimental setups such as the CEREMA's Adverse Weather facility and the weather chamber at the JARI not only are they extremely expensive and require large spaces, but are also extremely complex to make as generating large volumes of fog having the required characteristics in terms of particle sizing and spatial uniformity is an extremely complex challenge [14]. On the contrary, the proposed method is extremely cheap and simple to implement. The main limitation is that, at present, it is not easy to exactly define the limits of applicability of the proposed method in terms of fog conditions and target distance.

As reported in section III, the proposed method made it possible to easily analyze the performance of a commercial LiDAR (the MRS 6000 model, by Sick). Although the results obtained are likely to have lower accuracy than that which

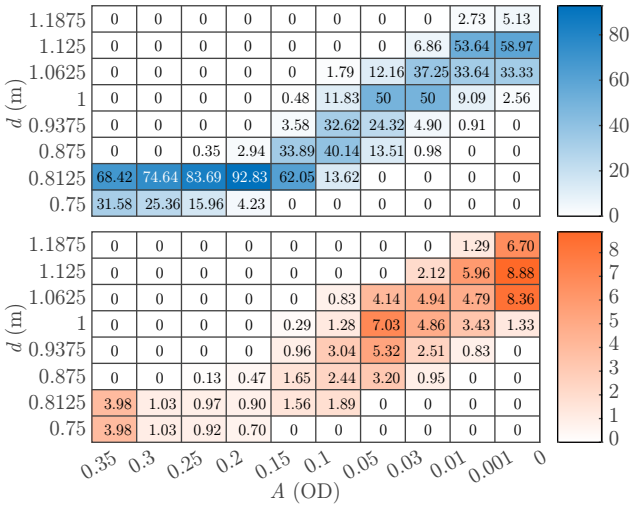

Fig. 5. $P(\%)$ (top) and $s(\%)$ (bottom) as a function of A.

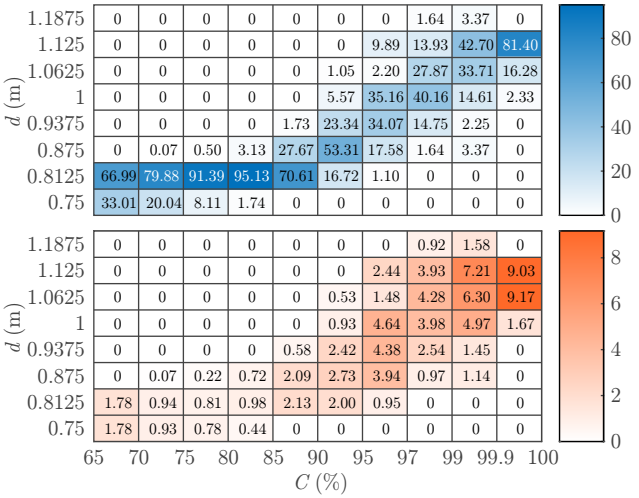

Fig. 6. $P(\%)$ (top) and $s(\%)$ (bottom) as a function of C.

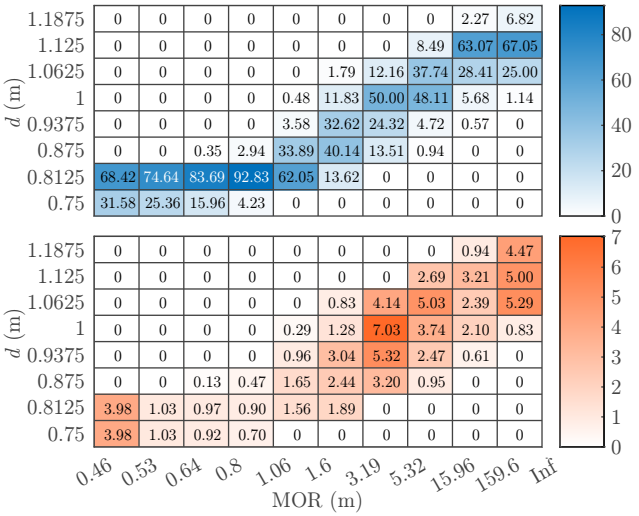

Fig. 7. $P(\%)$ (top) and $s(\%)$ (bottom) as a function of the MOR.

could be obtained using larger and more complex setups, they allow for quick and economical benchmarking of different LiDAR systems. In fact, the synthetic representations shown in Fig.s 5, 6 and, 7 allow to quickly compare the performances both in terms of absorbance and contrast. Furthermore, through the MOR, they also provide information of the performances as a function of the meteorological optical range, MOR. Note that the absorbance is calculated at the specific wavelength of the IUT. Hence, the same fog level can give rise to slightly different absorbances if the compared LiDARs have different wavelengths. The same is also true for the MOR. Conversely, the contrast is independent of the IUT wavelength. Thus, the absorbance and the MOR are more useful for analyzing the performances of the IUT, while the contrast allows a more immediate benchmarking.

REFERENCES

[1] F. Wang, Y. Zhuang, H. Gu, and H. Hu, "Automatic generation of synthetic LiDAR point clouds for 3-D data analysis," *IEEE Transactions on Instrumentation and Measurement*, vol. 68, no. 7, pp. 2671–2673, 2019.

[2] S. Cattini, L. Di Cecilia, L. Ferrari, and L. Rovati, "Optical characterization of the beams generated by 3D-LiDARs: proposed procedure and preliminary results on MRS1000," *IEEE Transactions on Instrumentation and Measurement*, vol. 69, no. 10, pp. 7796–7804, 2020. [Online]. Available: https://doi.org/10.1109/TIM.2020.2984137

[3] J. Lambert, A. Carballo, A. M. Cano, P. Narksri, D. Wong, E. Takeuchi, and K. Takeda, "Performance analysis of 10 models of 3D LiDARs for automated driving," *IEEE Access*, vol. 8, pp. 131 699–131 722, 2020.

[4] S. Cattini, D. Cassanelli, L. D. Cecilia, L. Ferrari, and L. Rovati, "A procedure for the characterization and comparison of 3-D LiDAR systems," *IEEE Transactions on Instrumentation and Measurement*, vol. 70, pp. 1–10, 2021.

[5] S. Cattini, D. Cassanelli, G. Di Loro, L. D. Cecilia, L. Ferrari, and L. Rovati, "Analysis, quantification, and discussion of the approximations introduced by pulsed 3D-LiDARs," *IEEE Transactions on Instrumentation and Measurement*, vol. 70, pp. 1–11, 2021.

[6] M. Rodriguez-Cortina, P. Adamiec, J. Barbero, X. Quintana, and M. A. Geday, "Emulation technique of multiple overlapped return echoes of a spatial LIDAR with 100-dB dynamic resolution," *IEEE Transactions on Instrumentation and Measurement*, vol. 70, pp. 1–7, 2021.

[7] M. Kutila, P. Pyykonen, H. Holzhuter, M. Colomb, and P. Duthon, "Automotive LiDAR performance verification in fog and rain," in *2018 21st International Conference on Intelligent Transportation Systems (ITSC)*, 2018, pp. 1695–1701.

[8] WMO-N8, *Guide to Instruments and Methods of Observation*. World Meteorological Organization, 2018, vol. I - Measurement of Meteorological Variables. [Online]. Available: https://library.wmo.int/index.php?id=12407&lvl=notice_display

[9] ISO 28902-1:2012, "Air quality — Environmental meteorology — Part 1: Ground-based remote sensing of visual range by lidar," ISO — International Organization for Standardization, Geneva, Switzerland, Tech. Rep., 2012. [Online]. Available: https://www.iso.org/standard/45022.html

[10] H. Gross, *Handbook of Optical Systems*, 1st ed. Wiley, 2012, vol. 5, ch. 48: Radiometry.

[11] V. E. Zuev, *Propagation of Visible and Infrared Radiation in the Atmosphere*. John Wiley & Sons, 1974. [Online]. Available: https://archive.org/details/nasa_techdoc_19720022686

[12] S. Cattini and L. Rovati, "Low-cost imaging photometer and calibration method for road tunnel lighting," *IEEE Transactions on Instrumentation and Measurement*, vol. 61, no. 5, pp. 1181–1192, May 2012.

[13] F. D. Shepard, *Reduced Visibility Due to Fog on the Highway*. National Cooperative Highway Research Program, NATIONAL ACADEMY PRESS, 1996. [Online]. Available: http://onlinepubs.trb.org/Onlinepubs/nchrp/nchrp_syn_228.pdf

[14] P. Duthon, M. Colomb, and F. Bernardin, "Fog classification by their droplet size distributions: Application to the characterization of Cerema's platform," *Atmosphere*, vol. 11, no. 6, 2020. [Online]. Available: https://www.mdpi.com/2073-4433/11/6/596